Electron-Beam Studies of Viscous Flow in Supersonic Nozzles

DIETMAR E. ROTHE*
Cornell Aeronautical Laboratory, Inc., Buffalo, N. Y.

Performance predictions for attitude control jets of satellites and manned spacecraft suffer from the lack of well-substantiated theoretical and experimental data in the fully viscous nozzle-flow regime. This paper presents an experimental investigation of the internal and external flow for nozzle Reynolds numbers in the general range between 10^2 and 10^3 with nitrogen as the test gas. Electron-beam techniques are used for measuring gas density and rotational temperatures at selected points throughout the flow. Discharge coefficients are also measured. In addition, some effects of ambient pressure on the external flow structure are studied by flow visualization experiments. At the lower Reynolds numbers studied, experimentally determined temperatures indicate the existence of a supersonic bubble inside the nozzle expansion cone, with a subsequent shock-free viscous transition to subsonic flow. These results substantiate the theoretical prediction of this phenomenon, first made by Rae in an earlier phase of this program.

I. Introduction

LOW-THRUST rocket engines are required for providing the small corrections necessary to maintain proper attitude and to make minor changes in the trajectory of orbiting satellites and deep-space planetary probes. Thrust levels are usually a fraction of a pound-force and may in some instances be as low as 10^{-6} lbf ($\approx\frac{1}{2}$ dyne). Small nozzle scale and low reservoir pressures combine to give throat Reynolds numbers in the range between 10 and 10^4. At the lower end of this range the viscous boundary layer is quite thick and tends to fill the entire cross section of the nozzle. Under these conditions an inviscid analysis followed by a boundary-layer correction is no longer adequate, especially when transition-flow characteristics, such as slip at the wall, have to be taken into account. Difficulties in predicting the thrust and mass flow levels that will occur in the vacuum of the space environment make the flight rating of these thrusters a very lengthy and expensive process. Frequently the uncertainty in nozzle performance causes a penalty in greater system complexity.

Few experimental data exist with respect to nozzle performance at Reynolds numbers less than 10^4. Available information is to a major part limited to gross characteristics such as thrust and discharge coefficients and contributes relatively little to an understanding of the flow structure itself. Discharge coefficients, for example, have been determined by Milligan[1] at throat Reynolds numbers between 10^{-1} and 10^3 and recently by Massier et al.[2] at Reynolds numbers between 10^3 and 10^6 for a few isolated geometries. A relatively detailed survey of static and total pressures throughout the flow in a nozzle, operating at a Reynolds number of approximately 10^3, has been reported by Yevseyev.[3] His work also includes a study of the effects of back pressure on the internal flow. A general review of microrocket technology prior to 1966 is given by Sutherland and Maes.[4]

Among several theoretical methods, which have been applied to low-density nozzle flows, the slender-channel formulation has been found to give an approximate description of the flow at Reynolds numbers applicable to microthrust rockets. The slender-channel equations were first used by Williams[5] in a similar-solutions analysis and were later applied by Rae,[6] who obtained general numerical solutions for several realistic nozzle configurations. The results of Rae's calculations, which were performed in an earlier phase of the present program, are generally consistent with the experimental pressures and Mach numbers reported by Yevseyev[3] at a Reynolds number of 10^3. The series of experiments described in the present paper was initiated for the purpose of substantiating some of the predictions made by Rae[6] at lower Reynolds numbers and for providing new data that may be used as a basis for formulating an improved version of this theory. For the sake of easy comparison with Rae's calculations, the Reynolds number B used here is identical with his and is defined by

$$B = \rho_o \hat{u} r_* / \mu_o \tag{1}$$

where ρ_o and μ_o are gas density and viscosity in the stagnation chamber. The symobl $\hat{u}$ represents the adiabatic escape speed, $\hat{u} = (2H_o)^{1/2}$, and r_* is the throat radius.

In the following section the electron-beam technique for determining static temperatures and densities in nitrogen is briefly reviewed. The instrumentation and experimental procedure are described in Sec. III. Results are presented and discussed in Sec. IV.

II. Electron-Beam Technique

Within the last decade the electron-beam fluorescence technique[7-12] has found general acceptance for determining gas densities and gas temperatures in low-density aerodynamic problems. With this method the thermodynamic properties of the gas are determined from an analysis of the electron-beam excited spectrum. In nitrogen flows, a suitable spectral feature is the 0,0 vibrational band (at 3914Å) of the first negative system of N_2^+, which results from transitions between the $B\,^2\sum_u^+$ state and the ground state of the ion. At low pressure levels (<0.5 torr), where collisional quenching effects are not important, and at gas temperatures below 800°K, the integrated intensity of this band is proportional to gas density. The rotational fine structure in this emission band is indicative of the relative number distribution of excited molecules among the rotational energy levels of the $B\,^2\sum_u^+$ state. If the statistical rules governing the excitation process from the neutral ground state to the $B\,^2\sum_u^+$ state are

Presented as Paper 70-810 at the AIAA 3rd Fluid and Plasma Dynamics Conference at Los Angeles, Calif., June 29–July 1, 1970; submitted August 17, 1970; revision received December 15, 1970. This research was sponsored by NASA under Contract NASW-1668. Technical direction was provided by F. E. Compitello of NASA Headquarters. Thanks are due W. J. Rae and P. V. Marrone for their contributions to this program.

* Research Aerodynamicist. Member AIAA.

understood, the original undisturbed population of the rotational energy levels in the gound state can be derived.

When a gas molecule absorbs a quantum of energy from a passing electron of kilovolt energy, the process of excitation, as a result of the rapidly changing electromagnetic field of the moving electron, is not unlike the excitation produced by the absorption of a photon. Consequently, it may be assumed that the optical selection rules can be applied to the electron-beam excitation process. This assumption was employed by Muntz,[8] who first suggested that the electron beam may be used to determine gas temperatures in nitrogen flows. He showed that the method gives accurate temperature measurements in the range between 300°K and 400°K. Experiments performed subsequently in expanding flows of nitrogen by Robben and Talbot,[9] Marrone,[10] Ashkenas,[11] and Petrie and Boiarski[12] have shown that even very low temperatures can be determined in supersonic flows by the electron-beam method, provided the following conditions exist. 1) The flow is expanding at a rate slow enough and at densities high enough for the rotational degrees of freedom to remain in equilibrium with translational random energies. 2) The radiation analyzed derives from excited molecules that have been produced by collisions with high-energy electrons only.

The second condition is necessary to exclude the effects of low-energy secondary electrons. For excitation by low-energy electrons (<200 ev) the optical selection rules are known to be violated (see, e.g., Polyakova et al.[13]), so that the method of interpretation used by Muntz[8] would indicate an apparent non-Boltzmann distribution of rotational energies. Since a fraction of the electron-beam luminescence is caused by low-energy secondaries (Harbour et al.[14]), produced in ionizing collisions of primaries with gas molecules, a small apparent deviation from Boltzmann behavior is generally observed. This is most pronounced for the rotational lines corresponding to higher rotational quantum numbers ($K > 10$). If this effect is ignored, the measured rotational temperatures are generally too high. The discrepancy is of the order of 10°K and is approximately constant over the temperature range of interest here. Petrie and Boiarski[12] have studied this effect under conditions where rotational freezing was absent, and have found that, if care is taken to observe the center of the electron beam only, and if the low-intensity lines in the tail of the band are excluded from the analysis, then the discrepancy does not exceed 5°K in the temperature range from 20°K to 300°K. Under these conditions, the effect of secondary electrons on the measured temperatures is negligible at room temperatures and becomes important only at extremely low temperatures. At static temperatures above 50°K the error amounts to less than 10%.

Band spectra obtained in the present experiments were analyzed as proposed by Muntz,[8] except that lines in the tail of the band which measured less than 10% of the maximum line intensity were omitted in the data reduction for reasons stated previously. For example, the data analysis was restricted to the first 13 lines at 200°K and to the first seven lines at 50°K. The information thrown away in the tail of the band pertains to a very small fraction of the total rotational energy in the gas, so that the temperatures calculated are still representative of the state of rotational excitation. Within the limits of this data analysis no deviation from Boltzmann behavior was observed, and the experimental temperatures obtained are believed to be within 5% of the actual gas temperatures.

III. Experimental Arrangement and Procedure

1. Instrumentation

All experiments were performed in the test section of a steady-flow low-density test facility, which has been described in detail elsewhere.[15] Measurements of gas density and temperature were obtained by the electron-beam technique outlined above.

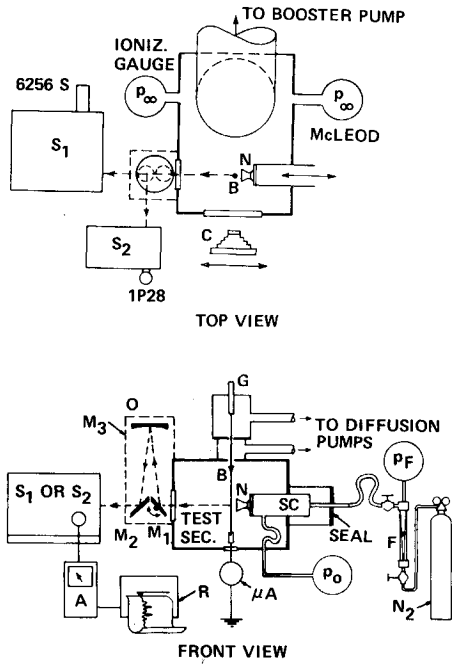

Fig. 1 Outline of experimental arrangement.

A beam of electrons (15 kv–100 μA) was produced by a differentially pumped electron gun G, which was mounted on top of the test section (Fig. 1). The electron beam was passed through different regions of the flow by moving the nozzle N with respect to the electron beam. Keeping the electron beam fixed in the laboratory frame of reference had the advantage that the optics required no realignment when the point of observation was shifted to a new position in the flowfield.

The nozzle and the stagnation chamber SC could also be translated at a uniform rate in the axial direction for flow visualization purposes. The structure of low-density nozzle plumes may be photographed by moving the electron beam relative to the flowfield in a plane defined by the beam and the flow axis, while taking a time exposure of the beam luminescence. Since the beam luminescence is everywhere proportional to the gas density, a density map of a two-dimensional flow section is recorded on the film by this procedure, which has been described in an earlier paper.[16] With the present arrangement, the nozzle and the camera C were moved at uniform and equal velocities relative to the stationary electron beam.

The electron-beam fluorescence was analyzed by two spectrometers, S_1 and S_2, which viewed the beam from the downstream direction (Fig. 1). The mirror M_2 could be rotated around a vertical axis to form an image of the electron beam in the entrance-slit plane of either instrument. The slits were masked, so that light entering the spectrometers was limited to radiation originating in a small volume of gas. The resulting spatial resolution was better than 1 mm in any direction. A test-section window of quartz was used to assure uniform transmission in the near ultraviolet.

Rotational temperatures were determined by analyzing the fine structure of the $N_2^+(0,0)$-band with a $\frac{3}{4}$ m scanning Czerny-Turner spectrometer, S_1 (Fig. 1). The instrument had an $f/6.5$ aperture and was used in second order, where the linear dispersion was 5Å/mm. An S-13 quartz-window photomultiplier served as the detector. The anode current was amplified by an electrometer A and recorded with an ink-pen recorder R.

Gas densities were measured with a low-dispersion Ebert-type spectrometer, S_2, which had an exit slit wide enough to

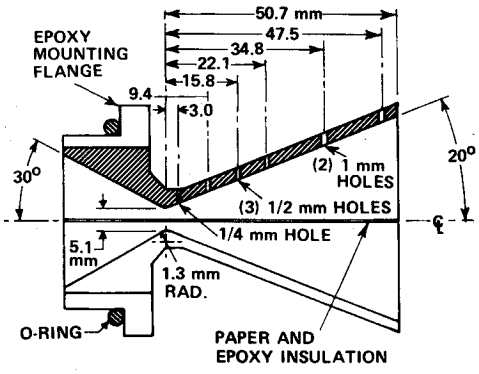

Fig. 2 Graphite nozzle (5 mm).

accept the entire $N_2^+(0,0)$-band. The entrance slit was perpendicular to the beam image produced by mirrors M_1 to M_3. This made the density measurements independent of beam spreading due to small-angle scattering.

With either instrument the point of observation could be moved up and down the electron beam by rotating the diagonal mirror M_1 around a horizontal axis (Fig. 1). This permitted densities and temperatures to be determined at off-axis points in the flow. Rotation of this mirror was controlled by a linkage and a motor-driven micrometer, such that the micrometer reading corresponded directly to position along the electron beam. Radial density profiles through the flow-field were obtained by moving the point of observation along the beam at uniform speed, while recording the total band intensity as a function of time.

2. Nozzles

For the study of low-density viscous nozzle flows, two geometrically similar graphite nozzles were built with throat diameters of 5 mm and 2.5 mm. Graphite was chosen because of its unique physical properties. Its black surface color reduced optical reflections inside the nozzle. Its thermal and electrical conductivity made it possible to use the nozzle as a beam collector. The low atomic number of carbon helped to minimize back-scattering and secondary emission of electrons, when the beam was terminated on or in the nozzle. The subsonic and supersonic portions of each nozzle were cones having half-angles of 30° and 20°, respectively (Fig. 2). Relatively sharp throats were used with longitudinal radii of curvature equal to $\frac{1}{4}$ the throat diameters (or $r_*/2$). The maximum area ratio at the exit was 66 for both nozzles.

Small holes were drilled through the top wall of each nozzle to permit the electron beam to enter the nozzle interior. The hole diameters decreased towards the throat and were less than two local molecular mean free paths for the majority of the present tests. Hence, the flow disturbance caused by these holes could be considered negligible. Each nozzle was built from two halves, which were electrically insulated from each other and from ground, so that the portion of the electron current intercepted by each half could be measured separately. This feature made it possible to optimize the alignment of a given hole with respect to the electron beam, and to determine the beam current inside the nozzle from the current collected by the bottom half of the nozzle.

When the electron beam was terminated inside the nozzle, and all the kinetic energy of the electron beam (1.5 w) was intercepted by the nozzle surfaces, the nozzle temperature could be expected to increase during long exposures to the beam. To prevent hot nozzle walls from influencing the measurements, only one density scan or temperature determination was performed at a time. The electron beam was then immediately turned off (or the nozzle was moved out from under it), and a high mass flow (>1 g/min) of nitrogen was passed through the nozzle for a minimum period of 10 min, to bring the wall temperatures back to the adiabatic equilibrium values before proceeding with the next measurement. The 10-min interval was found to be more than adequate, since variations in the cooling time produced no change in the gas temperatures measured near the wall.

Density profiles obtained inside the nozzle had to be corrected for back-scattering effects near the point of electron impact. Usually only the bottom half of a diametrical density profile was significantly affected. Corrections were never more than 20% and were determined from static calibration tests described elsewhere.[15,17] The remaining probable error in the density measurements is believed to be less than 5%.

IV. Results and Discussion

Temperature and density measurements were made throughout the flow inside nozzles, using nitrogen as the test gas and a stagnation temperature of $T_0 = 300°K$. Nozzle Reynolds numbers B ranged from 100 to 1500. Different Reynolds numbers were obtained by varying the pressure p_o in the stagnation chamber. The stagnation chamber pressures required for a specific value of B are given by

$$p_o = B/166 \text{ torr} \qquad (5 \text{ mm nozzle}) \qquad (2)$$

and by

$$p_o = B/83 \text{ torr} \qquad (2.5 \text{ mm nozzle}) \qquad (3)$$

A representative selection of these measurements is presented in Figs. 3–7. In the first series of tests care was taken to ensure that the ambient pressure (p_∞ = 2–10μ Hg) was always lower than the jet pressure at the nozzle exit, so that the plumes were underexpanded.

1. Centerline Temperatures

Temperature measurements at points on the centerline of the nozzle show a consistent pattern of change with Reynolds number. Except for the two bottom curves all data in Fig. 3 are experimental. The lower curve represents the ideal expansion, based on inviscid theory and the actual area change in the nozzle. As expected, the departure from inviscid theory becomes greater the smaller the Reynolds num-

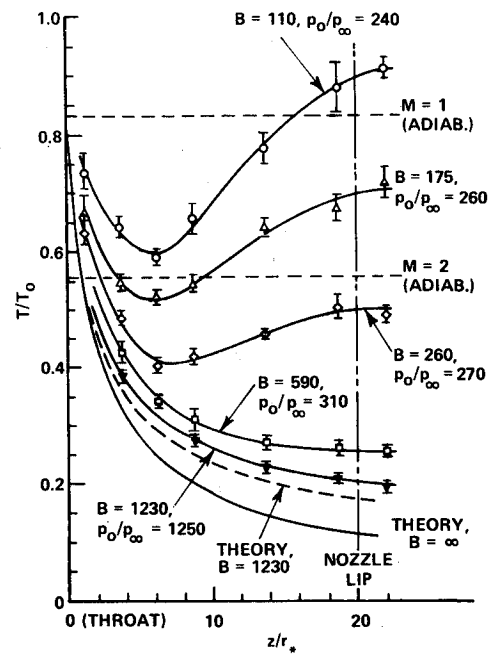

Fig. 3 Measured gas temperatures along nozzle axis for maximum nozzle pressure ratios (open symbols: 5-mm nozzle; filled symbols: 2.5-mm nozzle).

ber. The experimental error bars in Fig. 3 are random errors only and are based on the signal-to-noise ratio in the rotational spectra.

Two distinctly different types of behavior are observed. For $B > 500$ the axial temperatures decrease monotonically from throat to nozzle exit. For $B < 300$, on the other hand, the temperatures pass through a minimum near $z = 6r_*$ and then increase again towards the nozzle exit. The temperature increase is the result of thermalization of the flow energy due to viscous dissipation. It must, therefore, be accompanied by a decrease in velocity and Mach number. For $B = 110$, the temperatures determined near the exit lie above the sonic conditions for adiabatic flow. If cross-streamline heat conduction is considered to be of minor importance in this region, then the flow emerging from the nozzle may be regarded as subsonic. Hence, the flow in this case expands in the normal manner to supersonic velocities just downstream of the throat ($M \approx 1.8$ at $z = 5r_*$), but then reverts back to subsonic flow in a viscous shock-free transition. This type of behavior was predicted by Rae[6] for just this Reynolds number. The observation of this phenomenon represents strong support for the general validity of the slender-channel formulation.

A direct comparison of experiment with theory is given for $B = 1230$. The theoretical curve was calculated for the present nozzle geometry with the computer program developed by Rae. The agreement between experiment and theory is good to within 3%.

The temperature rise observed at low Reynolds numbers cannot be interpreted as a compression wave, since the experimental density and pressure are decreasing in this region of the expansion (Figs. 4 and 5). It is, therefore, not caused by an upstream effect of the ambient gas. As will be shown later, the basic shape of this temperature profile is not altered by the external gas pressure, as long as the plume remains underexpanded ($p_o/p_\infty \gtrsim 250$). The slowing down of a supersonic channel flow to subsonic speeds by viscous shear forces alone has not been observed before. The phenomenon is not altogether new, however, since such a transition takes place in all supersonic compressible boundary layers. In a nozzle it is associated with a frictional choking of the flow, insofar as a decrease in ambient pressure will not increase the mass

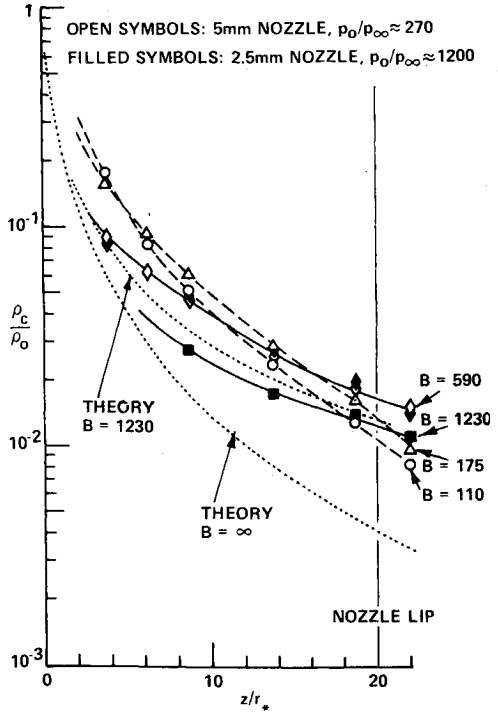

Fig. 4 Centerline densities at maximum nozzle pressure ratios.

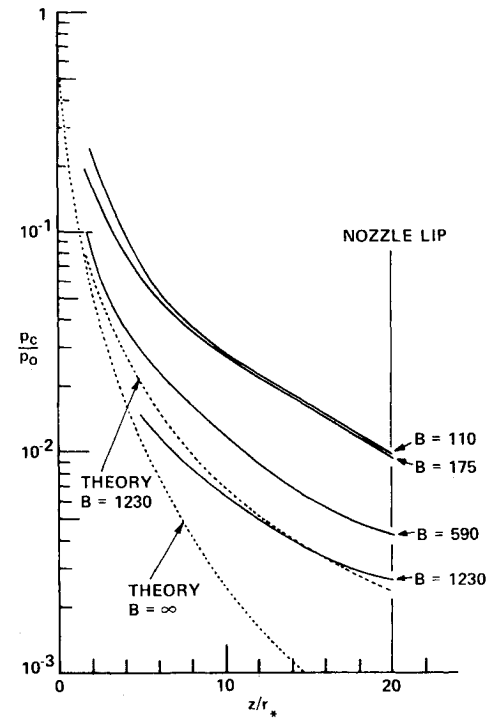

Fig. 5 Centerline pressures derived from measured densities and temperatures (Figs. 3 and 4).

flow passed by the nozzle, even when the entire flow is subsonic.

The possibility of rotational nonequilibrium occurring in the low-density nozzle flows has been considered.[15,17] Tests based on a sudden-freezing criterion[18] indicated that rotational freezing effects are negligible for any of the flows described here.

2. Densities and Pressures

Experimental centerline densities, ρ_c, corresponding to conditions discussed in Fig. 3 are given in Fig. 4. Again, there is evidence of two different types of behavior. Densities for $B > 500$ decrease in the expected manner (note theoretical curve for $B = 1230$) at a slower rate than predicted by inviscid theory. For $B < 200$ the negative density gradient is considerably steeper and exceeds the inviscid gradient near the nozzle exit.

For $B = 590$, density measurements were obtained with the 2.5-mm nozzle as well as with the 5-mm nozzle (Fig. 4), and the experimental values of ρ_c/ρ_o were found to be independent of nozzle size and nozzle pressure ratio (p_o/p_∞). This confirms that the results scale with B, and that there is no pronounced difference in the flow when p_o/p_∞ is raised from 300 to 1200. The latter is an indication that the experimental observations apply also to nozzles exhausting into a complete vacuum ($p_o/p_\infty \to \infty$).

Centerline pressures were derived from the measured temperatures and densities by making use of the equation of state for a perfect gas. These pressure curves (solid lines) are compared with theory (dotted lines) in Fig. 5. For the low Reynolds numbers the axial pressure profiles appear to converge to an asymptotic limit, at which the normalized pressures become independent of B. At Reynolds numbers below 100 the flow approaches isothermal, subsonic, near free-molecular conditions.

Representative radial density profiles are displayed in Fig. 6. Measured densities have been made dimensionless through division by the centerline density at each particular axial position z/r_*. Radial distance r is measured in units of the radial distance to the wall, r_W. The left half of Fig. 6 shows radial density profiles for $B = 110$. In this flow regime the

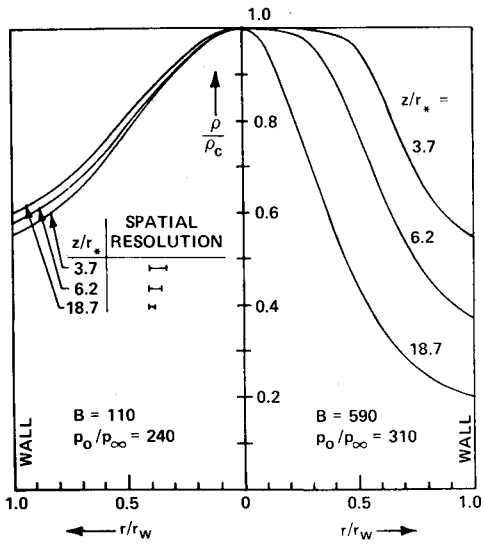

Fig. 6 Measured radial density profiles in the 5-mm nozzle at two different Reynolds numbers.

normalized density profiles are almost independent of axial position. The flow is fully viscous and exhibits no uniform core.

The right-hand side of Fig. 6 gives the corresponding profiles for $B = 590$. Near the throat at $z/r_* = 3.7$ a small inviscid core exists in this case. This inviscid core, however, shrinks to zero by the time the flow reaches the nozzle exit. In contrast to the low Reynolds number flow, the density profiles are distinctly nonsimilar here, indicating nonuniform entropy production[15,17] across the flow. For $B = 1230$ experimental density profiles[15] exhibit a small inviscid core, which persists right to the nozzle exit.

Off-axis temperatures were also measured for a limited number of experimental tests. Temperatures determined near the nozzle exit for $B = 590$ are plotted in Fig. 7. The corresponding density and pressure profiles are also given. As before, the pressures were calculated from the measured

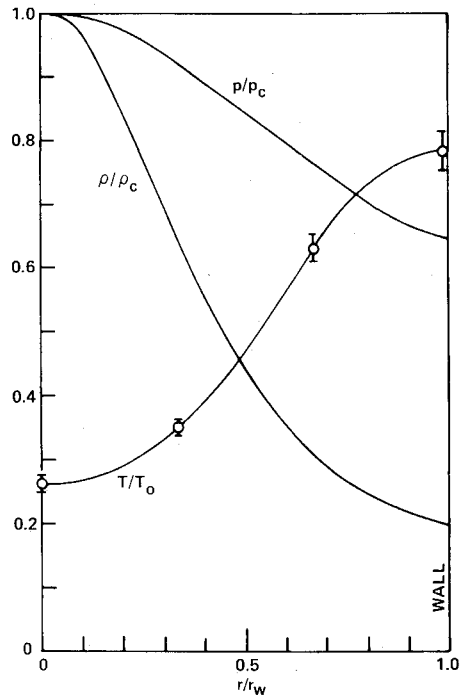

Fig. 7 Experimental variation of normalized temperature, density and pressure with radial distance near nozzle exit ($z/r_* = 18.7$, $B = 590$, $p_0/p_\infty = 310$).

temperatures and densities. The gas temperature near the wall is approximately 0.8 T_0, which is in agreement with the predictions made by Rae[6] for an adiabatic wall including slip at the boundary. The normalized temperature profile is not the exact inverse of the density profile, so that the pressure is not constant across the flow. In fact, the observed pressure at the wall is 35% lower than the centerline pressure. Radial pressure gradients of this magnitude have also been observed[15] at other Reynolds numbers. At Reynolds numbers near 100 the wall pressures are approximately 40% lower than pressures near the axis. This suggests that the slender-channel theory may not be entirely adequate to describe the flow in a nozzle having a 20° expansion cone.

It may be noted that the radial gradients of density, temperature, and pressure do not vanish at the wall (Figs. 6 and 7). Because the radial coordinate makes an angle of 20° with respect to the normal to the boundary, small negative radial gradients are expected near the wall corresponding to the radial components of the tangential gradients. The radial pressure gradient observed at the wall is consistent with a zero normal pressure gradient. However, the data indicate that there exist nonzero density and temperature gradients in a direction normal to the adiabatic wall. This indicates the noncontinuum character of the flow in this Reynolds number regime. The exact density gradients at the wall could not be determined, because of the finite spatial resolution of the measurements (horizontal bars in Fig. 6).

It is of interest here that the jet plume for the flow described in Fig. 7 was the least underexpanded one of this experimental series. At the exit, the ambient pressure p_∞ was below the pressure at the center but was above the pressure at the wall. The observed radial pressure distribution is thus evidently not caused by the low ambient pressure, but may have to be considered a characteristic feature of low Reynolds number expansions in nozzles. To check for possible flow separation in this case, the gas properties near the wall were determined along the length of the expansion cone. No evidence of flow separation was detected.

3. Effect of Ambient Pressure

Microthrust nozzles find applications in free space, yet have to be tested and flight-rated in the laboratory. Unless a space simulation chamber with an enormous pumping capacity is available, it is difficult to maintain a high vacuum, when even a small steady mass flow (10^{-3} to 10^{-1} g/sec) must be accommodated. It is therefore of interest to determine how low-density nozzle flows are affected by nonzero ambient pressures, and how low this pressure has to be for effective space simulation to be possible. At high Reynolds numbers ($>10^5$) the supersonic portion of the flow fills almost the entire cross-sectional area at the exit, apart from a thin boundary layer, and the flow in the nozzle and in parts of the plume is effectively isolated from the ambient conditions by shock waves

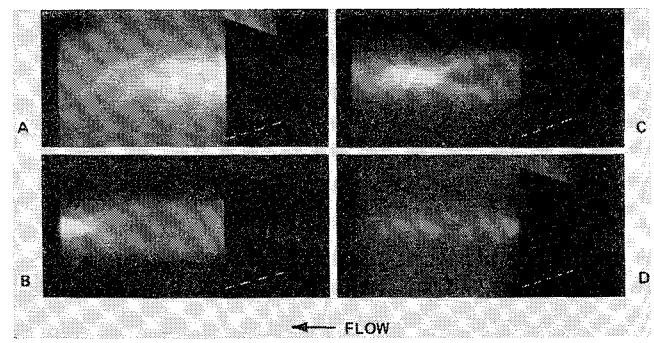

Fig. 8 Flow visualization photographs showing flow separation at low p_0/p_∞ (high ambient pressure); A) $B = 450$, $p_0/p_\infty = 310$; B) $B = 1550$, $p_0/p_\infty = 325$; C) $B = 1550$, $p_0/p_\infty = 185$; D) $B = 1550$, $p_0/p_\infty = 55$.

originating at the nozzle lip. Under these conditions the internal flow remains undisturbed, whether the flow is highly underexpanded or slightly overexpanded. However, at low Reynolds numbers the supersonic region is often restricted to a narrow core, and external conditions are able to influence the internal flow through the thick subsonic boundary layer.

A brief survey of this problem was conducted by flow visualization of external plumes and by sample temperature measurements in the nozzle and in the plume. For a given Reynolds number, different pressure ratios p_o/p_∞ were obtained by keeping p_o constant and changing p_∞. The ambient pressure was varied by throttling the booster pump of the tunnel. A series of photographs showing the plume structure for different nozzle pressure ratios is shown in Fig. 8. The flow was made visible by the method discussed in Sec. III. Regions of high luminosity represent regions of relatively high gas density. The nozzle is at the right, and the flow is from right to left. The external and internal diameters at the nozzle mouth are 48 mm and 42 mm, respectively. Figure 8A shows a slightly underexpanded jet obtained at $B = 450$ and $p_o/p_\infty = 310$. There is very little structure in this jet. The flow fills the whole nozzle, and the density in the plume drops off gradually in all directions. This type of flowfield is representative of all the flows discussed earlier for which temperatures and densities were determined.

At a Reynolds number of $B = 1550$, a nozzle pressure ratio of approximately 300 is no longer sufficient to produce an underexpanded plume (Fig. 8B). Here, the relatively high ambient pressure (28μ Hg) has caused flow separation inside the nozzle. The supersonic core is enveloped by a barrel-shaped shock wave, which originates in the expansion cone of the nozzle. As seen from the beam luminosity, the region surrounding the barrel shock appears to be occupied by stagnant gas at the ambient pressure. As the ambient pressure is increased (p_o/p_∞ decreased), the point of flow separation moves further upstream in the nozzle (Figs. 8C and D), and the plume shows a repetitive pattern of expansion diamonds, which shrink in size as p_o/p_∞ decreases. In Fig. 8D the first diamond is entirely within the nozzle. The work of Love et al.[19] has shown that this pattern of expansion diamonds occurs only when the jet pressure at the plume origin is less than twice the ambient pressure. Hence, it is concluded that, for cases shown in Figs. 8B–D, flow separation occurs at a point where the static pressure in the flow has dropped to a value of approximately 2 p_∞. From this point on, the presence of the nozzle wall is superfluous and has no influence on the jet plume, since the flow does not follow it.

When the centerline temperature near the nozzle exit (T_E) is monitored as a function of p_o/p_∞, the behavior shown in Fig. 9 is observed. The point of observation E lies one throat diameter downstream of the nozzle exit. The lower curve in Fig. 9 was obtained at a nozzle Reynolds number of 590. In the region where the plume is underexpanded at the exit ($p_o/p_\infty > 200$), no change in T_E is observed when p_o/p_∞ is changed from 1000 to 200. In this range of pressure ratios, the ambient pressure has, therefore, little or no influence on the expansion in the nozzle. As p_o/p_∞ is decreased further,

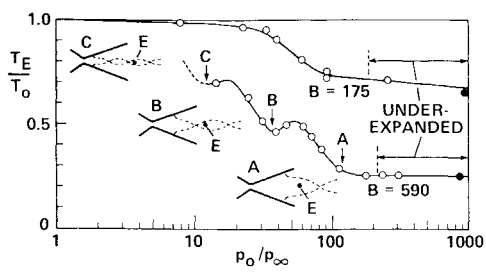

Fig. 9 Jet temperature just downstream of nozzle lip as a function of ambient pressure p_∞ (point E is on axis and $2r_*$ beyond exit plane; open symbols: 5-mm nozzle; filled symbols: 2.5-mm nozzle).

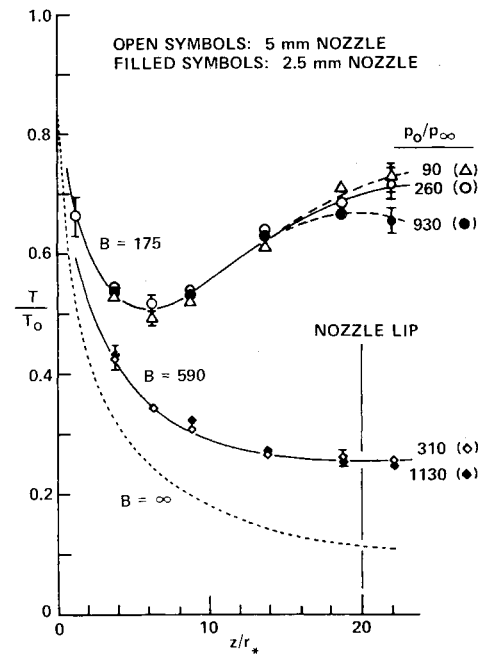

Fig. 10 Effect of ambient pressure on centerline temperatures.

however, T_E rises and falls in a cyclic manner, which correlates with the observed plume patterns described above. As the ambient pressure rises, the shrinking diamond pattern moves through the point E. At A this point lies within the first diamond; at B and C it lies inside the second and third expansion cells, respectively. Eventually, as p_o/p_∞ approaches unity, the flow remains subsonic throughout the nozzle, and T_E approaches T_o.

This cyclic behavior is not observed in the fully viscous flow regime. At $B = 175$ the exit temperature increases monotonically as p_o/p_∞ is decreased from 10^3 to below 10. Most of the change occurs for pressure ratios between 10^2 and 10. However, even for underexpanded pressure ratios ($p_o/p_\infty > 200$) a possible small variation of T_E with p_o/p_∞ was observed. These measurements indicate that there exists a possible upstream influence due to the ambient pressure at very low Reynolds numbers. To investigate this upstream influence, axial temperatures were measured throughout the nozzle at several pressure ratios.

For $B = 175$ such measurements were performed for pressure ratios ranging over more than an order of magnitude from 90 to 930 (Fig. 10). Most of the adjustment in the axial temperatures, over the underexpanded range of pressure ratios, was found to take place outside the nozzle; although some influence is observed at points which lie several molecular mean free paths inside the nozzle. The fundamental shape of the temperature curve remains unaltered, however, so that the profiles of Fig. 3 can indeed be considered as representative for the entire underexpanded range. No measurable change in any of the centerline temperatures was observed for $B = 590$ as p_o/p_∞ was varied by a factor of four (Fig. 10).

4. Discharge Coefficients

Measured mass flow rates were used to calculate discharge coefficients C_D for the nozzles and flow conditions studied. The discharge coefficient for a nozzle is defined as the actual mass flow divided by the ideal inviscid mass flow. The values of C_D obtained are plotted as a function of B in Fig. 11. These range from 0.9 at $B = 1000$ to approximately 0.75 at $B = 100$. In addition to the present values, the diagram also contains discharge coefficients predicted by Rae[6] and previous experimental values by Massier et al.[2] and by Milligan.[1]

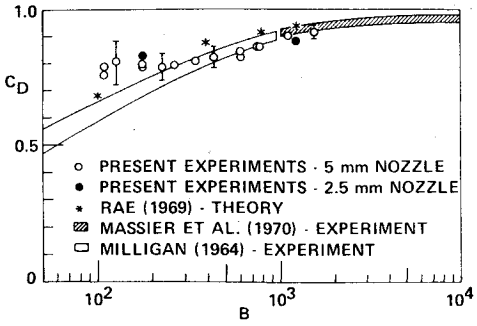

Fig. 11 Measured discharge coefficients compared with previous data.

There only exists an approximate agreement between all of the data. Specific comparisons are not possible, because the nozzle configurations and operating conditions were all different. Previous experimental data were obtained at relatively small wall angles (10°) and at very low pressure ratios. The pressure ratio for a choked nozzle flow is not expected to affect C_D at large Reynolds numbers. At $B < 500$, however, some influence of p_o/p_∞ on C_D would be expected. The deviation of the present data from Milligan's measurements may well be a result of the difference in the experimental pressure ratios.

V. Summary

The electron-beam technique has been extended to the study of internal nozzle flows at Reynolds numbers between 100 and 1500. Point measurements of gas temperature and density were made in nozzles that have a relatively sharp throat and a conical supersonic section with a 20° wall angle. The expanding flows were found to exhibit two different types of behavior, each characteristic of a particular Reynolds number range.

For $B > 500$ a small inviscid core was found to exist in the flow. This core extends all the way to the nozzle exit at Reynolds numbers approaching 1000. In this range of B, centerline temperatures decrease monotonically from the throat to the exit, and the axial density and pressure gradients become less steep with lower Reynolds number. Radial density profiles are dissimilar along the length of the nozzle.

For $B < 300$ the flow is fully viscous with no indication of any isentropic core. Centerline temperatures first decrease, but then increase again towards the nozzle exit. The increase in temperature is brought about through conversion of directed flow energy into thermal energy by the action of the viscous shear stresses. Density and pressure keep decreasing in the region where the temperature rises. In fact, at these values of B, the centerline densities fall off faster with distance than they do at higher Reynolds numbers. Radial density profiles are approximately similar throughout the nozzle. For $B \approx 100$, temperatures measured at the exit indicate subsonic flow, even though supersonic flow exists further upstream. This substantiates the prediction by Rae[6] of a supersonic bubble embedded in the expanding flow at this Reynolds number.

Over the entire Reynolds number range studied, significant negative radial pressure gradients were found to exist throughout the nozzle. Under conditions for which the flow near the exit is underexpanded, these gradients are believed to be insensitive to ambient pressure levels. At $B = 600$, experimental wall pressures are approximately 30% lower than pressures near the axis, whereas at Reynolds numbers near 100 the wall pressures are 40% lower. This feature should be taken into account when formulating an improved version of the theory.

A survey of back-pressure effects on the flow in the nozzle showed that flow separation occurs well upstream of the nozzle exit when the external pressure exceeds the static jet pressure near the exit. Under these conditions, the plume resembles that of a slightly underexpanded freejet originating at the point of separation in the expansion cone of the nozzle. When the ambient pressure is less than the nozzle exit pressure, however, the gas properties along the centerline appear to be insensitive to changes in the back pressure. Nozzles destined for space operation must be tested at sufficiently low ambient pressure to ensure underexpanded exit conditions. For $B < 300$, even lower ambient pressures may be necessary to eliminate all back-pressure effects.

The experiments discussed here have produced a significant gain in the understanding of viscous flows in nozzles, and ducts. Flow peculiarities predicted by the slender-channel theory have been observed, and ways for improving the theory have been pointed out.

References

[1] Milligan, M. W., "Nozzle Characteristics in the Transition Regime between Continuum and Free Molecular Flow," *AIAA Journal*, Vol. 2, No. 6, June 1964, pp. 1088–1092.

[2] Massier, P. F. et al., "Viscous Effects on the Flow Coefficient for a Supersonic Nozzle," *AIAA Journal*, Vol. 8, No. 3, March 1970, pp. 605–607.

[3] Yevseyev, G. A., "Experimental Investigation of Flow of Rarefied Gas," *AN SSSR. Izvestiya Mekhanika*, Moscow 1965, No. 3, pp. 165–172; Machine Translation in MT-67-22 (AD662502), March 31, 1967, AF Foreign Technology Div.

[4] Sutherland, G. S. and Maes, M. E., "A Review of Micro-rocket Technology: 10^{-6} to 1 lbf Thrust," *Journal of Spacecraft and Rockets*, Vol. 3, No. 8, Aug. 1966, pp. 1153–1165.

[5] Williams, J. C., "Viscous Compressible and Incompressible Flow in Slender Channels," *AIAA Journal*, Vol. 1, No. 1, Jan. 1963, pp. 186–195.

[6] Rae, W. J., "Some Numerical Results on Viscous Low-Density Nozzle Flows in the Slender-Channel Approximation," *AIAA Journal*, Vol. 9, No. 5, May 1971, pp. 811–820.

[7] Schumacher, B. W. and Gadamer, E. O., "Electron Beam Fluorescence Probe for Measuring the Local Gas Density in a Wide Field of Observation," *Canadian Journal of Physics*, Vol. 36, No. 6, June 1958, pp. 659–671.

[8] Muntz, E. P., "Static Temperature Measurements in a Flowing Gas," *The Physics of Fluids*, Vol. 5, No. 1, Jan. 1962, pp. 80–90.

[9] Robben, F. and Talbot, L., "Measurements of Rotational Temperatures in a Low Density Wind Tunnel," *The Physics of Fluids*, Vol. 9, No. 4, April 1966, pp. 644–652.

[10] Marrone, P. V., "Temperature and Density Measurements in Free Jets and Shock Waves," *The Physics of Fluids*, Vol. 10, No. 3, March 1967, pp. 521–538.

[11] Ashkenas, H., "Rotational Temperature Measurements in Electron-Beam Excited Nitrogen," *The Physics of Fluids*, Vol. 10, No. 12, Dec. 1967, pp. 2509–2520.

[12] Petrie, S. L. and Boiarski, A. A., "The Electron Beam Diagnostic Technique for Rarefied Flows at Low Static Temperatures," *Proceedings of the Sixth International Symposium on Rarefied Gas Dynamics*, Vol. II, 1969, M.I.T., Cambridge, Mass., pp. 1685–1701.

[13] Polyakova, G. N., Fogel, Y. M., and Zats, A. V., "Rotational and Vibrational Energy Level Distributions of N_2^+ Ions Produced in Collisions between Electrons and Nitrogen Molecules," *Soviet Physics JETP*, Vol. 25, No. 6, Dec. 1967, pp. 993–997; translated from *Journal of Experimental* and *Theoretical Physics* (USSR), Vol. 52, June 1967, pp. 1495–1503.

[14] Harbour, P. J., Bienkowski, G. K., and Smith, R. B., "Influence of Secondary Electrons on an Electron-Beam Probe," *The Physics of Fluids*, Vol. 11, No. 4, April 1968, pp. 800–803.

[15] Rothe, D. E., "Experimental Study of Viscous Low-Density Nozzle Flows," AI-2590-A-2, June 1970, Cornell Aeronautical Lab., Inc., Buffalo, N. Y.

[16] Rothe, D. E., "Flow-Visualization Using a Traversing Electron Beam," *AIAA Journal*, Vol. 3, No. 10, Oct. 1965, pp. 1945–1946.

[17] Rothe, D. E., "Electron-Beam Studies of Low Reynolds Number Flows inside a DeLaval Nozzle," AIAA Paper 70-810, Los Angeles, 1970.

[18] Lefkowitz, B. and Knuth, E. L., "A Study of Rotational Relaxation in a Low-Density Hypersonic Free Jet by Means of Impact-Pressure Measurements," *Proceedings of the Sixth International Symposium on Rarefied Gas Dynamics*, Vol. II, 1969, M.I.T., Cambridge, Mass., pp. 1421–1438.

[19] Love, E. S. et al., "Experimental and Theoretical Studies of Axisymmetric Free Jets," TR R-6, 1959, NASA.

MAY 1971 AIAA JOURNAL VOL. 9, NO. 5

Some Numerical Results on Viscous Low-Density Nozzle Flows in the Slender-Channel Approximation

WILLIAM J. RAE*
Cornell Aeronautical Laboratory, Buffalo, N.Y.

Calculated results are presented for converging-diverging nozzle flows in which viscous effects are important across the entire nozzle cross section. The slender-channel equations are used, with slip boundary conditions at the walls. The solution is started upstream of the throat, using asymptotic results for slow viscous flow in a converging cone. An implicit finite-difference scheme is then used to calculate the pressure, and profiles of velocity and enthalpy at successive stations along the channel. The cases chosen for presentation show the effects of varying the nozzle geometry, the Reynolds number, and the thermal condition of the nozzle wall. The results suggest that specific impulse is improved by a throat whose longitudinal radius of curvature is small, and that exit area ratios as low as ten can be used without serious loss of performance. It is shown that, at sufficiently low Reynolds numbers and low exit-cone angles, there is no solution of the slender-channel equations in which the flow can expand to supersonic conditions. Instead, the boundary layer closes, and the solution resembles a viscous subsonic pipe flow. The implications of this finding on the upstream influence of the exit-plane conditions and on the limits of validity of the slender-channel equations are discussed.

Nomenclature

a = speed of sound
A = $\dot{m}/2\pi\rho_0(2H_0)^{1/2}r_*^2$
A/A_* = geometric area ratio
B = $\rho_0(2H_0)^{1/2}r_*/\mu_0$
D = ρ/ρ_0
F = thrust
$\bar{F}$ = $F/p_0\pi r_*^2$
h = static enthalpy
H = total enthalpy
$\dot{H}$ = $\sigma_w^2\int_0^1 \eta DU(\Theta + U^2)d\eta$; see Eq. (25)
k = thermal conductivity
$\dot{m}$ = mass flow rate
M = Mach number
$\mathfrak{M}$ = molecular weight
p = pressure
P = p/p_0
Pr = Prandtl number
Q = $(1/B)[\Theta^\omega(\partial/\partial\eta)(\Theta/Pr + U^2)]_{\eta=1}$ heat transfer from the wall to the gas corresponds to $Q > 0$
r,z = cylindrical coordinates
r_1 = longitudinal radius of curvature of the nozzle wall, at the throat
r_* = transverse radius of the nozzle throat
$\mathfrak{R}$ = universal gas constant
$R(z)$ = transverse radius of nozzle wall
R_1 = r_1/r_*
T = temperature
u,v = axial and radial velocity components
U,V = $u/(2H_0)^{1/2}$, $v/(2H_0)^{1/2}$
W = $V - U\eta d\sigma_w/dx$
x,σ = z/r_*, r/r_*
α_u,α_T = accommodation coefficients for velocity and temperature
γ = specific-heat ratio
δ_1 = displacement thickness
η = σ/σ_w
θ = wall angle
θ_1,θ_2 = entrance and exit cone angles, Sec. IV
Θ = h/H_0
μ = viscosity
ρ = density
σ = r/r_*
ω = exponent in viscosity, enthalpy relation
$(\ )_e$ = conditions at nozzle-exit plane
$(\ )_0$ = conditions in reservoir
$(\ )_W$ = conditions at the wall
$(\ )_\mathfrak{C}$ = conditions on the axis
$(\ )_*$ = conditions at the geometric throat

Presented as Paper 69-654 at the AIAA Fluid and Plasma Dynamics Conference, San Francisco, Calif., June 16–18, 1969; submitted March 13, 1970; revision received December 18, 1970. Research sponsored by NASA under Contract NASW-1668. Technical direction was provided by M. Curtis of the Goddard Space Flight Center and F. E. Compitello of NASA Headquarters; their advice and encouragement are gratefully acknowledged. The author is also grateful to his colleagues J. A. Lordi and P. V. Marrone for many discussions of this work, and to J. R. Moselle for his very capable handling of the computer programming.

* Principal Research Engineer, Aerodynamic Research Department. Member AIAA.

I. Introduction

THE rocket engines that are used for satellite attitude control are often required to produce a thrust less than one pound-force, extending in some instances to values as low as